

# Microfluidic Continuous Approaches to Produce Magnetic Nanoparticles with Homogeneous Size Distribution

Ane Larrea, Victor Sebastian, Manuel Arruebo, Jesus Santamaria

**Abstract**—We present a gas-liquid microfluidic system as a reactor to obtain magnetite nanoparticles with an excellent degree of control regarding their crystalline phase, shape and size. Several types of microflow approaches were selected to prevent nanomaterial aggregation and to promote homogenous size distribution. The selected reactor consists of a mixer stage aided by ultrasound waves and a reaction stage using a  $N_2$ -liquid segmented flow to prevent magnetite oxidation to non-magnetic phases. A milli-fluidic reactor was developed to increase the production rate where a magnetite throughput close to 450 mg/h in a continuous fashion was obtained.

**Keywords**—Microfluidics, magnetic nanoparticles, continuous production, nanomaterials.

## I. INTRODUCTION

THE precise control over the synthesis conditions of magnetic nanoparticles (MNPs) have received considerable attention from researchers in recent years [1]. This control governs the resulting nanoparticle physicochemical properties, crystallinity, colloidal stability, and success in the wide variety of feasible applications where MNPs can be used. Their unique properties in terms of chemical stability, size-dependent magnetic properties, high surface area per volume ratio, biocompatibility, low price and good magnetic response make these materials ideal for a wide variety of applications related to biomedicine: drug delivery, magnetic fluid hyperthermia, magnetic resonance imaging (MRI), tissue engineering and repair, biosensing and biochemical separations or sorting. For instance, for pharmaceutical and biomedical purposes, MNPs should possess an appropriated size depending on their envisaged application and narrow size distribution together with high magnetization values as well as an optimal surface coating to assure biocompatibility. MNPs for biomedical applications in therapy and diagnosis should also possess a combination of properties including [2]: (a) high magnetization for effective signal enhancement or high specific absorption rate, (b) appropriate size with uniform dispersion and appropriated surface functionalization for extended blood circulation times in either passive or active targeting, (c) easy surface

functionalization suitable for further chemistry and/or for specific uptake and internalization in cells, and (d) dispersibility in physiological media as well as biocompatibility.

The main synthesis pathways designed for the preparation of MNPs comprise physical and wet-chemical methods [1]. Wet-chemical methods are generally considered the most efficient route since it can be achieved a high control on crystallinity and physicochemical properties. However, this route implies the use of surfactants (i.e., microemulsions) to direct the synthesis to the desired shape and size, high temperature when using solvothermal processes, a fine pH control when using precipitation techniques and a controlled atmosphere which promotes the formation of a specific magnetic phase. High temperatures usually result in rapid nucleation and faster growth of the newly formed magnetic nanoparticles, which requires an excellent control of reactant mixing to obtain monodisperse and pure nanomaterials. Then, the lack of control during the synthesis on mixing and heat transfer can promote a heterogeneous distribution of sizes and shapes as well as the formation of different magnetic phases. Furthermore, these strict requirements during the synthesis of MNPs pose serious challenges for their mass production, and it implies that new and reproducible synthesis approaches to produce biocompatible and functionalizable MNPs are highly desirable [3]. Large scale production can be also achievable by using physical methods but, in those cases, the sizes of the resulting MNPs are difficult to control and also the resulting products are usually obtained in their powdered form, therefore, preventive actions are needed to avoid accidental exposure to them via the inhalatory route.

Magnetite ( $Fe_3O_4$ ) is the most commonly used MNP in the biomedical field for its high saturation magnetization and superparamagnetism when monodomain state and easy surface functionalization or grafting to assure biocompatibility. The synthesis of  $Fe_3O_4$  MNPs can be accomplished using two essential chemical routes: (a) co-precipitation of an alkaline mixture of  $Fe^{3+}$  and  $Fe^{2+}$  salt solutions in 2:1 molar ratio, respectively, under pH controlled conditions and (b) the oxidative hydrolysis of a  $Fe^{2+}$  salt in basic solution with a mild oxidant. The synthesis of  $Fe_3O_4$  nanostructures is usually carried out under air-free conditions to prevent the transformation of the  $Fe_3O_4$  into non-magnetic  $\alpha-Fe_2O_3$  by oxidation at high temperatures. Magnetite can also be oxidized at low temperatures to its allotropic antiferromagnetic or weakly ferromagnetic (at room temperature) form named

A. L., V.S., M. A. and J. S. are with the Department of Chemical Engineering. Aragon Institute of Nanoscience (INA), University of Zaragoza, Campus Río Ebro-Edificio I+D, C/ Poeta Mariano Esquillor S/N, 50018-Zaragoza, Spain (e-mail: victorse@unizar.es).

V.S., M. A. and J. S. are with the CIBER de Bioingeniería, Biomateriales y Nanomedicina (CIBER-BBN), C/ Monforte de Lemos 3-5, Pabellón 11 28029 Madrid.

maghemite ( $\gamma\text{-Fe}_2\text{O}_3$ ) [4]. Co-precipitation reactions of Fe(II) and Fe(III)-hydroxides are thermodynamically driven and do not provide good control over size distribution and crystallinity of the resulting particles [2], and non-pure magnetic phases with a poorly defined morphology and large size distribution can be obtained [5]. In co-precipitation reactions the pH plays the role of controlling the formation, growth and crystallization of the desired magnetic phase [6]. Alternatively, the oxidative hydrolysis method seems to address the shortcomings of the co-precipitation method [7].

Microfluidic systems are a powerful high-throughput tool to study and optimize a wide range of chemical reactions [8], and their use in the synthesis of nanoparticles is attracting a remarkable attention since their inherent properties [3]. Compared to conventional batch synthesis strategies, microfluidic systems allow a more precise control of the reaction conditions (reaction time, temperature, reactants concentration and stoichiometry) due to their high surface-area-to-volume ratios and that temperature and concentration gradients are avoided, which can lead to reductions in the resulting nanoparticle polydispersity, as well as to assure a specific crystal structure and the consequent control in the physicochemical properties and reproducibility in mass production.

Here, we present an extremely reliable approach to direct the fast synthesis of magnetic nanomaterials by controlling the reaction environment. Pure and crystalline magnetic phase of monodisperse magnetite nanoparticles was achieved in a time scale of 6 minutes. In this work we show that the selection of the proper microfluidic approach has been considered as a key variable to tune the magnetic phase and crystallinity during the synthesis process. A milli-fluidic reactor was designed to scale-up the continuous production of those MNPs, obtaining a high MNPs throughput. These findings are of high relevance since this microfluidic platform enables the production of MNPs on demand and on site, which is highly requested in biomedical and pharmaceutical applications.

## II. EXPERIMENTAL SECTION

### A. Chemicals

Potassium nitrate ( $\geq 99\%$   $\text{KNO}_3$ , Fluka), Ferrous sulfate heptahydrate ( $\geq 99\%$ ,  $\text{FeSO}_4 \cdot 7\text{H}_2\text{O}$ , Aldrich), Sodium hydroxide ( $\geq 98\%$   $\text{NaOH}$ , Aldrich), L-lysine crystallized ( $\geq 98\%$   $\text{C}_6\text{H}_{14}\text{N}_2\text{O}_2$ , Aldrich) and Sulfuric acid (95-98%,  $\text{H}_2\text{SO}_4$ , Aldrich) were used as received without further purification.

### B. Methods

#### 1. Synthesis of Lysine- $\text{Fe}_3\text{O}_4$ MNPs: Batch and Continuous Processes

The synthesis protocol used was based on the well-known oxidative hydrolysis reported elsewhere [9] but modifying the stabilizing agent in order to promote the MNP biocompatibility as briefly described here. The iron salt,  $\text{FeSO}_4$ , was precipitated in basic media ( $\text{NaOH}$ ) with a mild oxidant ( $\text{KNO}_3$ ). In the batch synthesis approach with the aid

of a mechanical mixer, a 40 mL solution of 0.1 M  $\text{KNO}_3$ , 90 mM  $\text{NaOH}$  and 1 mM of L-Lysine was prepared using deionized water. Afterwards, this solution was bubbled with argon during 15 minutes to remove any trace of dissolved oxygen. Subsequently, 4,4 mL of an aqueous solution containing 65 mM  $\text{FeSO}_4 \cdot 7\text{H}_2\text{O}$  and 17 mM of  $\text{H}_2\text{SO}_4$  was added dropwise under constant stirring. When the addition was completed, argon was allowed to pass for another 15 minutes and the resulting suspension was heated at  $90^\circ\text{C}$  for 1 hour in an oil bath.

In the continuous synthesis approach, solutions were prepared as follows. In a 60 mL vessel (solution 1), a solution consisting of 180 mM  $\text{KNO}_3$ , 162 mM  $\text{NaOH}$  and 1,85 mM L-lysine was prepared. Solution 2, was composed of: 60 mL of deionized water, 13 mM ferrous sulfate heptahydrate and 3,38 mM sulfuric acid. Argon was bubbled in each solution for 15 minutes. After deoxygenation, each solution was placed in 60 mL plastic Becton Dickinson syringes and injected in the microfluidic system by a Harvard Syringe Pump.

To produce iron oxide nanoparticles using the continuous flow synthesis, solutions 1 and 2 were injected at a proper flow rate to obtain the desire residence time according to the microfluidic system volume. Solution 1 and 2 streams were mixed in a PEEK polymer Y-junction (500  $\mu\text{m}$  ID) under a constant flow ratio of 1:1 in order to be able to use a unique syringe pump. The microfluidic system is composed of two PTFE coils (1/16" OD and 0.04" ID) which are conceived as mixing and reaction stages, respectively. According to the type of mixing or reaction stage selected, four different approaches were followed to control the magnetic nanoparticle synthesis, named as follows (Fig. 1): a) Mixing by internal diffusion. b) Mixing by liquid segmentation. c) Mixing by ultrasonic vibration. d) Mixing by ultrasonic vibration and reaction with a gas segmented flow. A liquid single phase was selected to promote both, reactants mixing by internal diffusion and the reaction itself. Silicone oil was injected after the PEEK Y-junction to accelerate the reactants mixing by a liquid-liquid segmented flow. The flow-rate ratio of the immiscible streams was equal to 1. Mixing by sonication was carried out setting the mixing PTFE coil in an ultrasonic bath and maintaining the bath temperature in the range of 25 and  $30^\circ\text{C}$  using a cooling bath. Finally, a new modification from the previous approach was established, adding a gas ( $\text{N}_2$ ) stream after the mixing coil to obtain a stable gas-liquid segmented flow in the reaction stage. The temperature at the reaction stage was varied from 70 to  $110^\circ\text{C}$ . Experiments with a synthesis temperature higher than  $90^\circ\text{C}$  was carried out maintaining the reactor pressure at 1.4 bar using a back pressure regulator. The synthesized nanoparticles were centrifuged at 10.000 rpm for 10 minutes, then washed twice with distilled water and finally re-suspended in distilled water.

The synthesis in the milli-reactor was carried out following the same procedure than in the microreactor, but the mixing and reaction stages consist of PTFE tubing of DI=1.6mm. Solution 1 and 2 streams were mixed in a PEEK polymer Y-junction of 500  $\mu\text{m}$  ID under a constant flow ratio of 1:1 in order to be able to use a unique syringe pump. The total

volume flow was 1.87 ml/min.

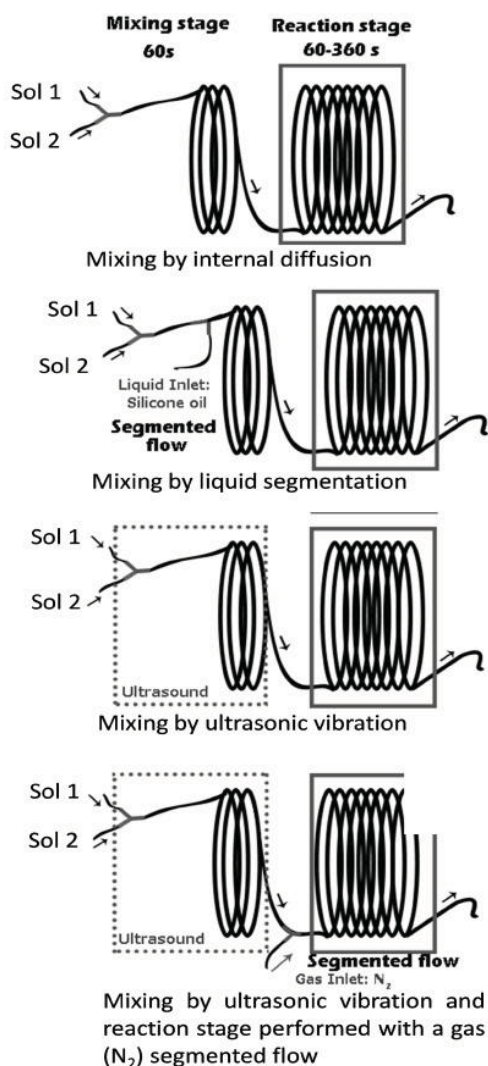


Fig. 1 Schemes of the microfluidics set-up designed to produce MNPs in continuous flow

### III. RESULTS AND DISCUSSION

The reported procedures to produce magnetite by the well-known oxidative hydrolysis method, implies the precipitation of an iron salt in basic media with a mild oxidant under an inert environment. The synthesis time required to obtain a crystalline and pure magnetite phase is 24 hours at a temperature of 90°C [7]-[9]. This synthesis time is out of the range of applicability of microfluidic reactors, where residence time in microfluidics is usually under the hour range. As starting point, we tried to reproduce the oxidative hydrolysis protocol [9] in a batch reactor at 90°C using a synthesis time of 1 hour under mechanical stirring. TEM images (Fig. 2) and electron-diffraction analysis (results not shown here) show that under those conditions a mixture of different magnetic species was obtained and then, 1 hour reaction time might not be enough for the complete

transformation of  $\text{Fe}^{2+}$  into  $\text{Fe}_3\text{O}_4$  NPs. This finding is in full agreement with some reported data [10], although in this case a different chemical composition in the reaction mixture was used.

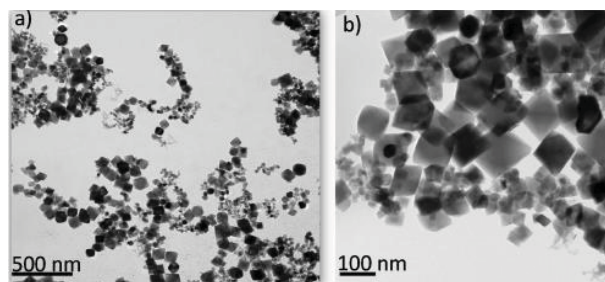


Fig. 2 TEM micrographs of magnetic nanoparticles obtained by mechanical mixing in a batch type reactor. Synthesis conditions: 90°C – 1h

In the microfluidic system here described, two aqueous solutions were mixed in a Y-junction, considering that the mixing time [11] ( $\tau_{\text{mix}}$ ) required for the complete mixing of the two inlet streams is 60 s (the effect of the chemical reactions involved was not considered), two microfluidic sections were set (Fig. 1): stage 1) mixing of precursors at room temperature and 60s residence time, stage 2) oxidative hydrolysis reaction at a temperature range between 70 and 110°C and a tunable residence time.

Preliminary experiments, carried out under 80°C and 300 s residence time, gave rise at the outlet of the reaction section (stage 2) a black dispersion with magnetic properties. The black color is representative of the transformation of  $\text{Fe}^{2+}$  into MNPs. However, the nanoparticle size distribution was very broad (Fig. 3). A careful observation at the mixing stage showed that the iron precursor precipitation was so fast that it immediately formed aggregates which were flowing randomly through the microtubing reactor. The residence time of these aggregates was not necessarily corresponding with the typical residence time distribution of a parabolic flow at laminar regime [12]. Then, new mixing approaches were proposed to control the formation of aggregates and to narrow the residence time distribution of the resulting MNPs including: i) to promote the flow segmentation with a non-miscible liquid (Fig. 4); ii) to irradiate the mixing stage with ultrasonic waves (Fig. 5).

Silicone oil was selected as continuous phase in the liquid-liquid segmented flow and discrete droplets of reagents were homogeneously formed. Despite the good mixing achieved at the slugs by the internal circulation [12], aggregates of few micrometers were still formed, although the aggregates were flowing along inside discrete droplets. The particle-size distribution of the resulting nanoparticles when using liquid segmentation was slightly narrower compared to the results obtained with the non-segmented flow but the improvement was not as much as it was expected (Fig. 4). In addition, a pure phase of spinel nanoparticles was unable to obtain under the different range of conditions tested. However, the



irradiation of the chemical reagents by ultrasonic waves at the mixing stage avoided the formation of aggregates of micrometric scale and then, the time spent by nanoparticles at the reaction stage of the microfluidic reactor was homogeneously distributed. TEM images confirm that the residence-time distribution was narrowed, since the particle-size distribution and shape of the obtained MNPs were practically similar (Fig. 5).

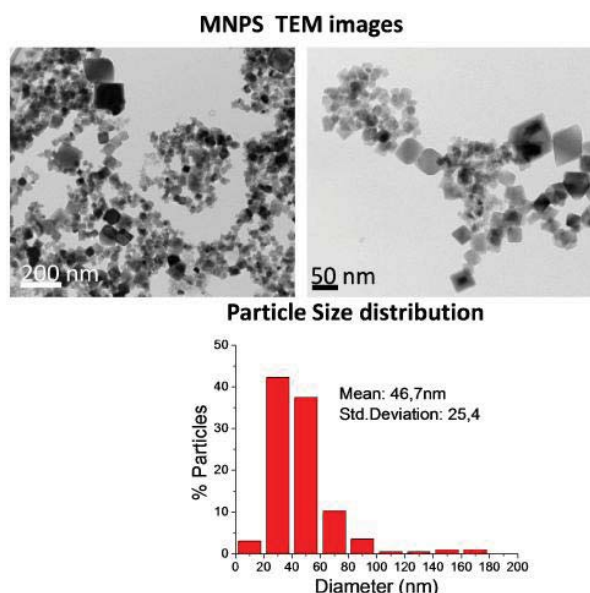


Fig. 3 Transmission electronic microscopy images and particle size distribution for MNPs obtained at the outlet of set-up where mixing was carried out by internal diffusion. Reaction stage: 100°C and 360s

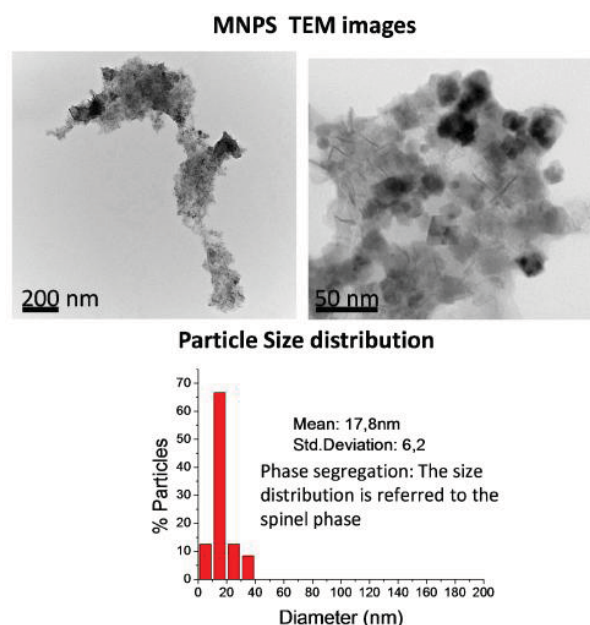


Fig. 4 Transmission electronic microscopy images and particle size distribution for MNPs obtained at the outlet of set-up where mixing was carried out by liquid segmentation. Reaction stage: 100°C and 360 s

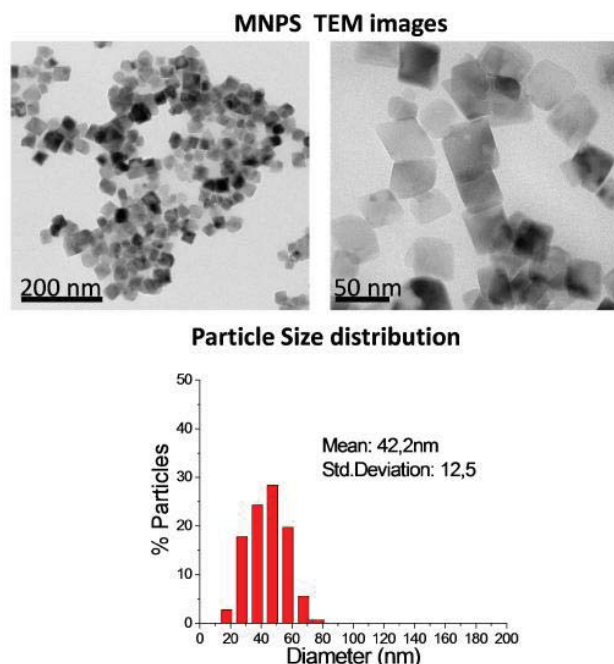


Fig. 5 Transmission electronic microscopy images and particle size distribution for MNPs obtained at the outlet of set-up where mixing was carried out by ultrasonic vibration. Reaction stage: 100°C and 360 s

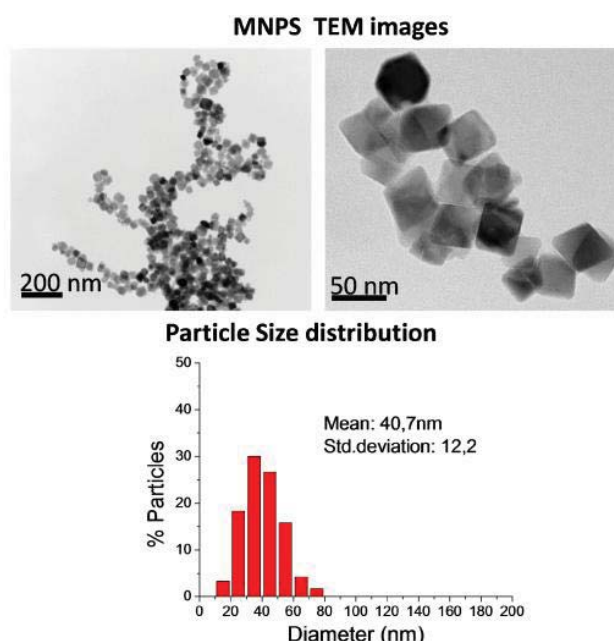


Fig. 6 Transmission electronic microscopy images and particle size distribution for MNPs obtained at the outlet of set-up where mixing was carried out by ultrasonic vibration and reaction stage performed with a gas ( $N_2$ ) segmented flow. Reaction stage: 100°C and 360 s

Particle-size measurements by transmission electron microscopy show that the particle-size deviation is slightly narrower when using the microfluidic reactor compared to the batch reactor, but, as an important improvement, in the

microfluidic reactor the MNPs were obtained in residence times as short as 6 minutes, over the 24 h reported for the batch mode [7]-[9]. Then it seems that the excellent control achieved by the microfluidic system in the heat and mass transfer processes during the nucleation-growth steps enables to decrease considerably the time required for a complete transformation of  $\text{Fe}^{2+}$  ions in  $\text{Fe}_3\text{O}_4$  spinel MNPs. To gain knowledge about the importance of the residence time and the reaction temperature on the quality of the MNPs, a variety of experiments varying the residence times at the reaction stage from 60s to 360s and the reaction temperatures from 80°C to 120°C were designed. MNPs morphology and particle-size measurements by TEM images showed that for a residence time as short as 60s, MNPs with the typical spinel-octahedral shape of magnetite phase [7] were obtained as a pure phase only at a reaction temperature higher than 100°C (Fig. 7). A mixture of ferric hydroxides (ferrihydrite and ferrihydrite), metastable magnetic phases with less ordered structures than magnetite, were obtained at reaction temperatures below 100°C. Under a residence time of 1 minute, the amount of ferric hydroxide decreased compared to the synthesis at high temperatures. On the other hand, if the residence time at the reaction stage was increased up to 6 minutes, the temperature required for the complete transformation of  $\text{Fe}^{2+}$  ions to the spinel was decreased as well (Fig 8.). The size distribution of the spinel nanoparticles did not significantly vary with the synthesis temperature. These growing evidences point out that the synthesis of magnetite NPs follow the classical nucleation and growth theory [13]. In fact, [14] demonstrated that nucleation and growth of magnetite proceed through a rapid agglomeration of nanometric primary particles.

The synthesis of magnetite nanoparticles ( $\text{Fe}_3\text{O}_4$ ) is usually directed under an inert atmosphere to prevent the oxidation and subsequent transformation of the spinel into maghemite ( $\gamma\text{-Fe}_2\text{O}_3$ ) in contact with air. Considering that the microfluidic reactor made of PTFE is slightly permeable to oxygen [15], we have modified the microflow distribution using a gas-liquid segmented flow to prevent the oxidation of magnetite during the continuous production. The liquid/gas flow ratio was kept constant at a value of 1 in order to achieve high recirculation, characterized by the vorticity, and to enhance the gas transfer to the liquid slug during the reaction stage. Nitrogen gas was injected into the microfluidic system just before the reaction stage at the proper conditions to support a steady gas-liquid segmented flow (Fig. 1). It could be observed during the MNP synthesis that as the liquid slugs were flowing through the reaction stage, the color of the suspension was turning into black. This supports the fact that  $\text{Fe}^{2+}$  ions are transforming into MNPs. The study on the influence of the residence time and temperature at the reaction stage revealed that a pure phase of magnetite could be only obtained at temperatures above 90°C (Figs. 6, 7). A residence time shorter than 6 minutes or a temperature lower than 90°C gave rise to a mixture of octahedral and laminar shaped nanocrystals which corresponds with magnetite and iron III hydroxides, respectively (Fig. 8) [16]. Consequently, the results achieved under  $\text{N}_2$  flow segmentation were practically

similar to the ones obtained without carrying the oxidative hydrolysis under an inert environment. This implies that the oxygen permeance through the PTFE tubing is not affecting the spinel growth since the residence time at the microfluidic system is short. However, the gas-segmented flow is more appropriate to avoid the oxidation of magnetite if  $\text{O}_2$  is not previously removed.

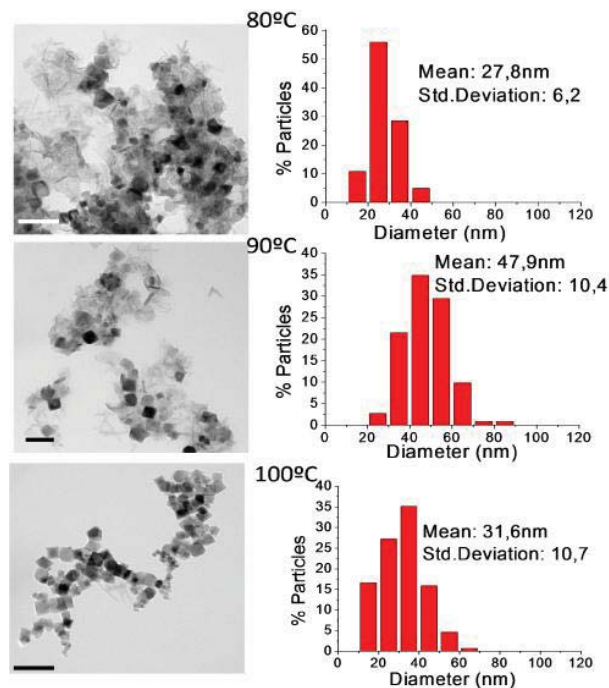


Fig. 7 TEM micrographs and particle size distribution of MNPs produced under ultrasonic vibration. Synthesis temperature and residence time at the reaction stage were varied from 80 to 110°C and 1 min, respectively. Scale bar: 100 nm

A high production scale-up was attempted in the continuous microfluidic system to demonstrate the suitability of microfluidic platforms to increase the production throughput. Flow uniformity, as well as reactants and residence time distribution must be maintained unchanged to preserve a good reactor performance after modifying the reactor from the microreactor to the millireactor scales [17]. Increasing the reactor volume by increasing the tubing length, while keeping the same tubing diameter, would result in both a high linear velocity and higher pressure drop. Under those conditions, it is well-known that the gas-liquid flow regime can be modified, obtaining annular, wavy annular or even churn flow [18], [19]. These flow modes promote the axial dispersion which is obviously an unwanted result in this work, since it could modify the particle-size distribution. Thus, we decided to scale-up the MNPs production by increasing both the reactor-tubing diameter and length. The aim was to maintain similar hydrodynamics that still provide an excellent control on transport rates and mixing [17]. Fig. 9 depicts the TEM image and particle-size distribution of the magnetite nanoparticles produced in the millireactor. It can be observed that the

millireactor is able to increase the production rate at the same synthesis conditions, obtaining the same quality in the resulting nanoparticles. In fact, the particle-size distribution is practically the same that the one obtained in the microreactor (Fig. 5). Regarding the production throughput, the millireactor used here enables to increase the production rate by approximately twenty-fivefold than the microreactor itself, which is an outstanding result (Table I).

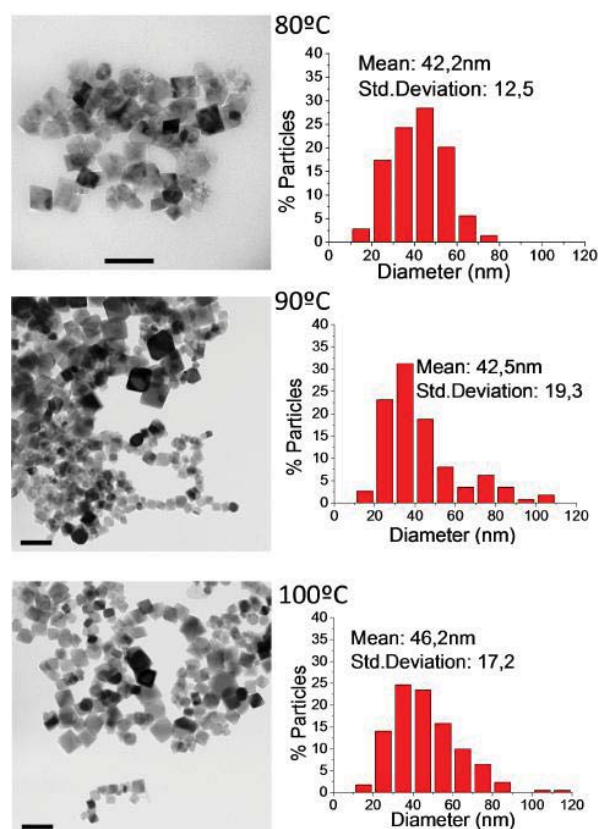


Fig. 8 TEM micrographs and particle size distribution of MNPs produced under ultrasonic vibration. Synthesis temperature and residence time at the reaction stage were varied from 80 to 110°C and 6 min, respectively. Scale bar: 100 nm

TABLE I  
MAGNETIC NANOPARTICLES PRODUCTION

Type of Reactor	Flow rate, $\mu\text{l}/\text{min}$	Production rate, $\text{mg}/\text{h}$
Microreactor	618	18.6
Millireactor	14960	449.0

Fig. 10 depicts the X-ray powder diffraction pattern from the magnetite nanoparticles obtained with  $\text{N}_2$  slug flow in the millireactor. All of the strong and sharp diffraction peaks in the XRD patterns can be indexed as the face center-cubic phase of  $\text{Fe}_3\text{O}_4$  products (JCPDS No. 19-0629). The diffraction pattern reveals that a highly pure phase of magnetite can be easily obtained at an extremely short synthesis time and in continuous mode.

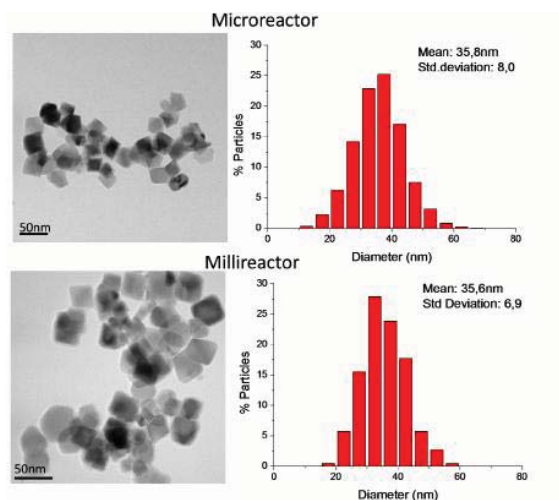


Fig. 9 TEM micrographs and particle-size distribution of MNPs produced in a micro and a millireactor under ultrasonic radiation and  $\text{N}_2$  gas-liquid segmented flow: residence time and synthesis temperature were 6 min and 90°C, respectively

The magnetic measurements carried out at different temperatures and the hysteresis loops for the resulting MNPs produced at the millireactor are shown in Fig. 10. A clear ferromagnetic behavior was obtained with a saturation magnetization close to 72 emu/g at 4 Tesla. The inset in Fig. 10 shows for this case a remanence of 8.4 emu/g and a coercivity of 80 Oe at 37°C. The resulting magnetization is very similar to the one obtained using a batch reactor where a saturation magnetization of 84 emu/g, a remanence of 15 emu/g and a coercivity of 115 Oe were obtained at 37°C but the synthesis in the microreactor took place in a few seconds instead of the hour needed to complete the synthesis in the batch reactor.

#### IV. CONCLUSION

In conclusion, the above results clearly show the potential of microfluidic systems to produce magnetic nanomaterials in ultra-fast times and continuous modes. A gas-slug microfluidic reactor was selected to synthesize high purity iron oxide magnetite nanostructures. Not only the productivity is enhanced by strongly reducing residence times with respect to the batch process (from hours to minutes), but also a high degree of control over the resulting product characteristics (size, shape, crystalline phase) can be obtained by simply changing the synthesis parameters. Our results show that it is beneficial to segregate the mixing and reaction stages. A fast mixing under ultrasound waves is essential, followed by a reaction stage with a fine tuning of temperature and residence time. This allows an accurate control on the final properties of the resulting products. In addition, a millireactor system was designed to increase the production rate, achieving a magnetite throughput of approximately 25-fold than the microreactor itself.



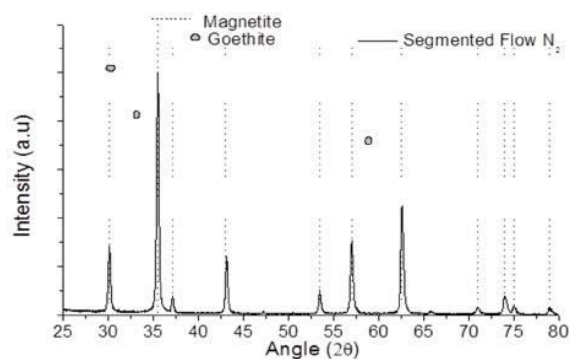


Fig. 10 X-ray powder diffraction patterns of MNPs obtained in the millireactor under  $N_2$  gas-liquid segmentation. Residence time and synthesis temperature were 6 min and 90°C, respectively

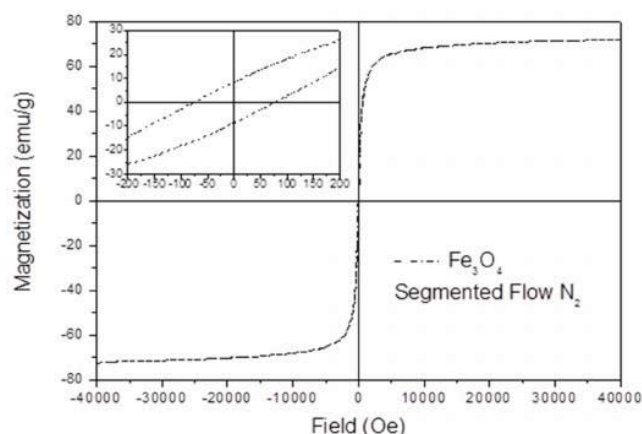


Fig. 11 Hysteresis loops (at 37 °C) of the magnetic nanoparticles produced in this work by using the millireactor: Insets in the top left corners show the region close to the (0,0) to show the coercivity and remanence. Residence time and synthesis temperature were 6 min and 90°C, respectively

#### ACKNOWLEDGMENTS

The EU CIG–Marie Curie under the REA grant agreement no. 321642 and the ERC Consolidator Grant program (ERC-2013-CoG-614715, NANOHEDONISM) are gratefully acknowledged.

#### REFERENCES

- [1] Reddy, L. H.; Arias, J. L.; Nicolas, J.; Couvreur, P. Magnetic Nanoparticles: Design and Characterization, Toxicity and Biocompatibility, Pharmaceutical and Biomedical Applications. *Chem Rev* 2012, 112, 5818-5878.
- [2] Xiao, L.; Li, J.; Brougham, D. F.; Fox, E. K.; Feliu, N.; Bushmelev, A.; Schmidt, A.; Mertens, N.; Kiessling, F.; Valldor, M.; Fadeel, B.; Mathur, S. Water-Soluble Superparamagnetic Magnetite Nanoparticles with Biocompatible Coating for Enhanced Magnetic Resonance Imaging. *Acs Nano* 2011, 5, 6315-6324.
- [3] Sebastian, V.; Arruebo, M.; Santamaria, J. Reaction Engineering Strategies for the Production of Inorganic Nanomaterials. *Small* 2014, 10, 835-853.
- [4] Correa, J. R.; Canetti, D.; Castillo, R.; Llopiz, J. C.; Dufour, J. Influence of the precipitation pH of magnetite in the oxidation process to maghemite. *Mater Res Bull* 2006, 41, 703-713.
- [5] Massart, R.; Cabuil, V. Effect of Some Parameters on the Formation of Colloidal Magnetite in Alkaline-Medium - Yield and Particle-Size Control. *J Chim Phys Pcb* 1987, 84, 967-973.
- [6] Jovanovic, S.; Spreitzer, M.; Otonicar, M.; Jeon, J. H.; Suvorov, D. pH control of magnetic properties in precipitation-hydrothermal-derived  $CoFe_2O_4$ . *J Alloy Compd* 2014, 589, 271-277.
- [7] Verges, M. A.; Costo, R.; Roca, A. G.; Marco, J. F.; Goya, G. F.; Serna, C. J.; Morales, M. P. Uniform and water stable magnetite nanoparticles with diameters around the monodomain-multidomain limit. *J Phys D Appl Phys* 2008, 41.
- [8] Marre, S.; Jensen, K. F. Synthesis of micro and nanostructures in microfluidic systems. *Chem Soc Rev* 2010, 39, 1183-1202.
- [9] Calatayud, M. P.; Riggio, C.; Raffa, V.; Sanz, B.; Torres, T. E.; Ibarra, M. R.; Hoskins, C.; Cuschieri, A.; Wang, L.; Pinkernelle, J.; Keilhoff, G.; Goya, G. F. Neuronal cells loaded with PEI-coated  $Fe_3O_4$  nanoparticles for magnetically guided nerve regeneration. *J Mater Chem B* 2013, 1, 3607-3616.
- [10] Iida, H.; Takayanagi, K.; Nakanishi, T.; Osaka, T. Synthesis of  $Fe_3O_4$  nanoparticles with various sizes and magnetic properties 14 by controlled hydrolysis. *J Colloid Interf Sci* 2007, 314, 274-280.
- [11] Nagy, K. D.; Shen, B.; Jamison, T. F.; Jensen, K. F. Mixing and Dispersion in Small-Scale Flow Systems. *Org Process Res Dev* 2012, 16, 976-981.
- [12] Cabeza, V. S.; Kuhn, S.; Kulkarni, A. A.; Jensen, K. F. Size-Controlled Flow Synthesis of Gold Nanoparticles Using a Segmented Flow Microfluidic Platform. *Langmuir* 2012, 28, 7007-7013.
- [13] Colfen, H.; Antonietti, M. Mesocrystals: Inorganic superstructures made by highly parallel crystallization and controlled alignment. *Angew Chem Int Edit* 2005, 44, 5576-5591.
- [14] Baumgartner, J.; Dey, A.; Bomans, P. H. H.; Le Coadou, C.; Fratzl, P.; Sommerdijk, N. A. J. M.; Faivre, D. Nucleation and growth of magnetite from solution. *Nat Mater* 2013, 12, 310-314.
- [15] Gomez, L.; Sebastian, V.; Irusta, S.; Ibarra, A.; Arruebo, M.; Santamaria, J. Scaled-up production of plasmonic nanoparticles using microfluidics: from metal precursors to functionalized and sterilized nanoparticles. *Lab Chip* 2014, 14, 325-332.
- [16] R. M. Cornell, U. S. The Iron Oxides: Structure, Properties, Reactions, Occurrences and Uses. WILEY-VCH; Weinheim, 2003.
- [17] Nieves-Remacha, M. J.; Kulkarni, A. A.; Jensen, K. F. Hydrodynamics of Liquid-Liquid Dispersion in an Advanced-Flow Reactor. *Ind Eng Chem Res* 2012, 51, 16251-16262.
- [18] Gunther, A.; Khan, S. A.; Thalmann, M.; Trachsel, F.; Jensen, K. F. Transport and reaction in microscale segmented gas-liquid flow. *Lab Chip* 2004, 4, 278-286.
- [19] Khan, S. A.; Gunther, A.; Schmidt, M. A.; Jensen, K. F. Microfluidic synthesis of colloidal silica. *Langmuir* 2004, 20, 8604-8611.